Journal of Power Sources 247 (2014) 831–839

Contents lists available at ScienceDirect

Journal of Power Sources

journal homepage: www.elsevier.com/locate/jpowsour

Characterization of Ni–YSZ anodes for solid oxide fuel cells fabricated by solution precursor plasma spraying with axial feedstock injection

Craig Metcalfe, Elisa Lay-Grindler, Olivera Kesler*

University of Toronto, Department of Mechanical and Industrial Engineering, 5 King's College Road, Toronto, Ontario M5S 3G8, Canada

HIGHLIGHTS

- Metal supported SOFC fabricated by plasma spraying with axial feedstock injection.
- Power density of 0.45 W cm^{-2} at 0.7 V was obtained at 750 °C.
- First performance result for SOFC anode fabricated by SPPS.
- Influence of processing parameters on anode composition investigated.

ARTICLE INFO

Article history:
Received 17 June 2013
Received in revised form
4 September 2013
Accepted 7 September 2013
Available online 18 September 2013

Keywords:
Solid oxide fuel cell (SOFC)
Anode
Nickel yttria-stabilized zirconia (Ni–YSZ)
Solution precursor plasma spraying (SPPS)

ABSTRACT

Nickel and yttria-stabilized zirconia (YSZ) anodes were fabricated by solution precursor plasma spraying (SPPS) and incorporated into metal-supported solid oxide fuel cells (SOFC). A power density of 0.45 W cm^{-2} at 0.7 V and a peak power density of 0.52 W cm^{-2} at 750 °C in humidified H_2 was obtained, which are the first performance results reported for an SOFC having an anode fabricated by SPPS. The effects of solution composition, plasma gas composition, and stand-off distance on the composition of the deposited Ni–YSZ coatings by SPPS were evaluated. It was found that the addition of citric acid to the aqueous solution delayed re-solidification of NiO particles, improving the deposition efficiency and coating adhesion. The composition of the deposited coatings was found to vary with torch power. Increasing torch power led to coatings with decreasing Ni content, as a result of Ni vaporizing in-flight at stand-off distances less than 60 mm from the torch nozzle exit.

1. Introduction

Metal-supported solid oxide fuel cells (SOFC) have the potential to reduce materials and manufacturing costs and to improve durability compared to electrode- and electrolyte-supported cells [1]. The metal support provides structure for the cell, allowing the electrodes and electrolyte to be thin, which has the potential to reduce materials costs. The use of a metal support also offers the potential for improved thermal shock resistance, which would allow for rapid start-up. Improved tolerance to thermal cycling of both tubular [2] and planar [3,4] metal-supported SOFCs has been demonstrated compared to that generally obtained with electrode or electrolyte supported cells.

Several processing methods have been used to fabricate metal-supported cells, as reviewed by Tucker [1]. Compared to methods requiring multiple infiltration and/or high temperature sintering steps, plasma spray processes, which do not require subsequent processing steps after deposition, offer the advantage of being a more rapid manufacturing method with increased throughput. Atmospheric plasma spraying (APS), compared to Vacuum plasma spraying (VPS), offers the additional advantage of fabrication under open atmosphere conditions, with a correspondingly lower equipment and operating cost. However, a significant challenge to the fabrication of SOFCs by plasma spray methods is the deposition of electrodes having both high surface area for electrochemical reactions and sufficient porosity for gas transport [5].

In conventional plasma spraying, the desired materials to be deposited are injected in dry powder form into the plasma. To avoid issues associated with feeding the powder to the torch, particles on the order of 10–100 μm are generally used. Such large particles can lead to a low surface area for electrode reactions in an SOFC. To obtain finely structured and porous coatings, primary particles on the micrometer or nanometer size scales may be agglomerated into larger particles, which may then be fed to the torch. This approach has been used previously for Ni–YSZ anodes [6]. The resulting

* Corresponding author. Tel.: +1 (416) 978 3835; fax: +1 (416) 978 7753.
E-mail addresses: tcm@mie.utoronto.ca (C. Metcalfe), elisa.lay@cea.fr (E. Lay-Grindler), kesler@mie.utoronto.ca (O. Kesler).

0378-7753/$ – see front matter © 2013 Elsevier B.V. All rights reserved.
http://dx.doi.org/10.1016/j.jpowsour.2013.09.035

coatings fabricated using nanostructured agglomerate feedstocks generally show a bi-modal structure [7,8], in which the core of the agglomerates retain their fine structure, while melting of the agglomerate surface leads to larger features.

Improving the microstructural homogeneity of plasma sprayed coatings coupled with a decrease in the average microstructural feature size would likely lead to improved performance of plasma sprayed SOFC electrodes. This objective has led to the application of liquid-based plasma spray processes [9] to the fabrication of SOFC electrodes [10,11]. Two different liquid based processes are currently under development in the literature, in which either a suspension of powders [12] or a solution containing precursors [13] for the desired materials to be deposited are injected into the plasma. These two processes are referred to as suspension plasma spraying (SPS) and solution precursor plasma spraying (SPPS), respectively.

The SPPS process has the potential to produce nanostructured coatings [14] without the difficulties of developing stable suspensions of NiO and YSZ powders. A promising feature of Ni–YSZ coatings fabricated by SPPS is that more uniform mixing between the Ni and YSZ phases is obtained, compared to that obtained using SPS [15]. There are, however, numerous properties of the solution feedstock that ultimately affect the coating properties, which must be understood for a particular coating application. These include the selection of precursor materials [16], their thermal decomposition characteristics in the plasma [13,17], their concentration in solution [18], and the choice of solvent. It is desired to have the precipitation of the precursor salts occur as close as possible to the torch exit [19] in order to mitigate the inclusion of incompletely synthesized material in the coating. It is also important to avoid precursors having endothermic decomposition processes, which could lead to cooler plasma temperatures and result in delayed formation of the desired phases [16]. If the metal oxide forms too far from the torch exit, there may not be sufficient plasma enthalpy to melt the material, resulting in poor deposition efficiency.

SPPS has been used to fabricate Ni–YSZ coatings [15,20,21] and a composite of Ni and La_2O_3 doped CeO_2 [22] for use as SOFC anodes; however, their electrochemical performance has not been reported. A hybrid method combining the SPS and SPPS processes has been developed and demonstrated at DLR [4], whereby nickel nitrate was added to a suspension of YSZ. In this study, the SPPS process is used to fabricate Ni–YSZ coatings for use as anodes in SOFCs. The objective is to understand the effects of solution composition, plasma gas composition, and stand-off distance on the composition and microstructure of the deposited Ni–YSZ coatings, fabricated using axial injection of the solution into the plasma. A metal-supported SOFC was fabricated, with the Ni–YSZ anode fabricated by SPPS, in order to evaluate its short-term electrochemical performance.

2. Experimental procedure

2.1. Plasma spray processing

All coatings were fabricated using an axial-injection APS system (Axial III, Series 600, Northwest Mettech Corp., North Vancouver, BC, Canada). Coatings were deposited on stainless steel supports having a 0.16 cm thickness and 2.54 cm diameter. Three different supports were used: polished non-porous 430 stainless steel discs were used for single stripe studies; porous 430 stainless steel discs (Media Grade 1, Mott Corporation, Farmington, CT, USA) were used for coating development; and porous stainless steel (1C44Mo20, Sandvik Osprey Ltd., Neath, UK) discs, containing 21–23 wt.% Cr, were pressed and sintered in-house and used for fuel cell fabrication. A fixture was used for preheating the substrates to 250 °C and cooling them upon reaching 400 °C, and a solution delivery system incorporating a Coriolis mass flow meter and peristaltic pump with pulse dampener was used to deliver the solution feedstock to the plasma torch. Both items are described in further detail in a previous work [23]. The solution was injected into the plasma using a stainless steel tube (0.84 mm internal diameter) centered within the torch convergence tube, through which nitrogen was used as an atomizing gas at a 30 slpm flow rate. Unless otherwise specified, the plasma torch was rastered over the stationary substrates at a speed of 42 cm s^{-1}.

2.1.1. NiO- and YSZ-forming precursors

Three different nickel salts were evaluated, including $Ni(NO_3)_2 \cdot 6H_2O$, $Cl_2Ni \cdot 6H_2O$, and $Ni(CH_3COO)_2 \cdot 4H_2O$, abbreviated Ni[n], Ni[Cl], and Ni[a] hereafter, respectively. To form $Y_{0.15}Zr_{0.85}O_{1.925}$, the precursors used were $Y(NO_3)_3 \cdot 6H_2O$ and $ZrOCl_2 \cdot 8H_2O$. All precursors were obtained from Alfa Aesar, Ward Hill, MA. Solutions were prepared with or without the addition of a combustible fuel species: anhydrous acetic acid (AA) was used for Ni[a] and citric acid (CA) monohydrate was used for Ni[n] and Ni[Cl]. All solutions used water as the solvent except when anhydrous acetic acid was used as both the combustible fuel species and solvent for Ni[a].

2.1.2. Fabrication of metal-supported button cell

The Ni–YSZ anode, YSZ electrolyte, and 60 wt.% $La_{0.6}Sr_{0.4}Co_{0.2}Fe_{0.8}O_{3-\delta}$ (LSCF) and 40 wt.% $Ce_{0.8}Sm_{0.2}O_{1.9}$ (SDC) composite cathode were deposited on a porous stainless steel support. The anode was deposited directly on the metal support using the conditions shown in Table 1. The electrolyte and cathode were subsequently deposited as described in previous works [6,23]. Note that insulating phases that have been reported to form at the interface between LSCF-containing cathodes and YSZ electrolytes during sintering [24] do not form during plasma spray processing [25].

2.2. Ex-situ heating of precursors

To evaluate the thermal characteristics of decomposition and oxide formation of each precursor, solutions were prepared and heated in air to 150 °C for 2 h, followed by a hold at 120 °C for approximately 12 h. The dried precursors were then heated in a simultaneous thermogravimetric analyser and differential scanning calorimeter (SDT-Q600, TA Instruments, New Castle, DE) at 10 °C min^{-1} in air flowing at 100 sccm. Approximately 10 mg of the dried precursor material was placed in an alumina crucible for each experiment.

2.3. Coating characterization

2.3.1. Single stripe studies

Images of deposits of NiO and YSZ from a single linear pass of the torch over the substrate were obtained from solution

Table 1
Plasma processing condition sets used.

Parameter	Conditions A	Conditions B	Conditions C
Plasma gas flow rate, slpm	200	225	225
Vol.% N_2	40	30–80	34
Vol.% Ar	55	Balance	61
Vol.% H_2	5	5	5
Current, A	570	600	600
Arc voltage, V	168	147–203	153
Torch power, kW	96	88–122	92
Stand-off distance, mm	60	60	60
Nozzle diameter, mm	7.9	9.5	9.5
Total feedstock flow rate, g min^{-1}	50	50	50

feedstocks both with and without citric acid addition to the solution. Ni[n] was used as the precursor for all runs involving Ni. Polished 430 stainless steel discs were mounted on a fixture rotating at 250 RPM, corresponding to a torch speed relative to the substrate of 380 cm s^{-1}. The substrates were pre-heated by passing the torch, without injecting feedstock, over the substrate 10 times at a linear speed of 4.2 cm s^{-1}. For each experiment, the flow rate of injected solution was adjusted such that the corresponding rate of solid formation was 2.4 g min^{-1}. After spraying, the metal discs were washed with water and images were obtained at 1.5 kV in a field emission scanning electron microscope (Hitachi S-4500) complemented by an Oxford Instruments High Purity Germanium energy dispersive x-ray spectroscopy (EDS) detector. For EDS analysis, an acceleration voltage of 20 kV was used.

2.3.2. Composition and phase

The composition of the composite coatings was evaluated by measuring the Ni mass fraction of the deposited coating. This was done by first heating the as-sprayed coating and substrate to 750 °C for 2 h in air to fully oxidize Ni metal and sub-stoichiometric nickel oxide to NiO, as well as to remove any insufficiently treated precursor material. The coatings were then heated to 600 °C for 4 h in 25 vol.% H_2, balance N_2, to reduce the NiO to Ni. The decrease in mass that occurred during the 600 °C heat treatment was attributed to the loss of oxygen resulting from the reduction of NiO to Ni, after correcting for oxidation of the metal support that occurs during plasma spraying and during the 750 °C heat treatment in air.

X-ray diffraction (XRD) measurements were performed using a Philips diffractometer (PW 1830 HT generator and PW 1050 goniometer, PANalytical B.V., Almelo, Netherlands) using Cu Kα radiation to determine the phases present in the coatings. XRD patterns were recorded using 0.02° and 2.0 s angular and time steps, respectively.

2.3.3. Deposition efficiency

Deposition efficiency (DE) was evaluated as the ratio of the mass of coating material deposited to the mass of material injected into the plasma while passing over the substrate. To avoid uncertainty in the mass of material deposited, coatings were first heat treated in air at 750 °C for 2 h prior to mass measurement such that the coating was composed only of NiO and YSZ, without Ni metal, sub-stoichiometric nickel oxide, or amorphous precursor material present.

2.4. Electrochemical testing

The fuel stream for electrochemical testing consisted of humidified H_2 (3 mol.% H_2O) flowing at 400 sccm, while the oxidant stream was air flowing at 1000 sccm. Electrochemical testing was performed using a Solartron 1470E multi-channel potentiostat and a 1260 frequency response analyzer (London Scientific, London, ON, Canada). Further details of the electrochemical test setup are described in a previous work [6]. Post-mortem imaging of the fuel cell cross section was performed by mounting the cell in epoxy under vacuum, sectioning with a precision diamond wafering blade, re-mounting in epoxy under vacuum, and subsequent grinding and polishing using 320 grit SiC paper and 9, 3, and 1 μm polycrystalline diamond suspensions, sequentially. Backscattered electron images were obtained using a scanning electron microscope (JSM6610, JEOL Ltd. Tokyo, Japan).

3. Results and discussion

3.1. Selection of precursors

Preliminary studies for selection of a suitable Ni precursor were made using aqueous 2 M solutions of Ni[n] or Ni[Cl] and a 0.6 M solution of Ni[a], as detailed in Table 2. The lower solubility of Ni[a] in water limited its concentration to 0.6 M. A concentration of 2 M was chosen to increase the likelihood of precipitation throughout the volume of each droplet over that of solutions with lower concentration [18]. An atomizing gas flow rate of 30 slpm, the full scale value of the installed mass flow controller, was used in order to decrease both the number averaged droplet diameter injected into the plasma and the droplet size distribution. A previous study, [26], using the same plasma torch convergence and injection tube, with 2 M solutions (total cation concentration) containing both Ni[n] and the same YSZ forming precursors used in this work, reported a decrease in the 50th percentile droplet diameter as well as a decrease in the difference between the 10th and 90th percentile droplet diameters with increasing atomizing gas flow rate. This result is consistent with that reported by Rampon et al. [27], in which an increase in the ratio of atomizing gas flow rate to suspension flow rate resulted in a decrease in the atomized droplet diameters. The aim was therefore to inject concentrated solutions with a narrow droplet diameter distribution and small droplet diameters in order to increase the likelihood of full-volume precipitation and to avoid shell formation, which has been shown to result in undesirable microstructural features [28].

Table 2
Solution composition for fabrication of NiO, YSZ, and NiO–YSZ coatings.

Parameter	Material(s) to be deposited			
	NiO	YSZ	NiO–YSZ (A)	NiO–YSZ (B)
Ni cation concentration, M	2.00[a]	–	2.00	2.20
Zr cation concentration, M	–	0.85	0.56	0.40
Y cation concentration, M	–	0.15	0.10	0.07
Citric acid concentration, M[b]	1.30	0.58	1.30	1.43
Solvent	Water[c]	Water	Water	Water

[a] When using Ni[Cl] and Ni[n]. 0.6 M Ni[a] was used in water. 1.0 M Ni[a] was used in acetic acid, due to the lower solubility of Ni[a].
[b] If present in solution.
[c] Unless otherwise specified.

Fig. 1 shows the DE obtained for different solutions containing each nickel precursor. The plasma processing conditions used to fabricate each coating are summarized under the heading Conditions A in Table 1. The Ni[Cl], Ni[a], and Ni[n] precursors resulted in DEs of 22%, 20%, and 9%, respectively; and the deposits were found to have a powdery nature, having poor adhesion to the substrate and poor cohesion of individual NiO particles making up the coating.

There are a number of mechanisms that could occur on their own or together to result in the observed low DE and poor adhesion of NiO fabricated from aqueous solutions. The NiO should be

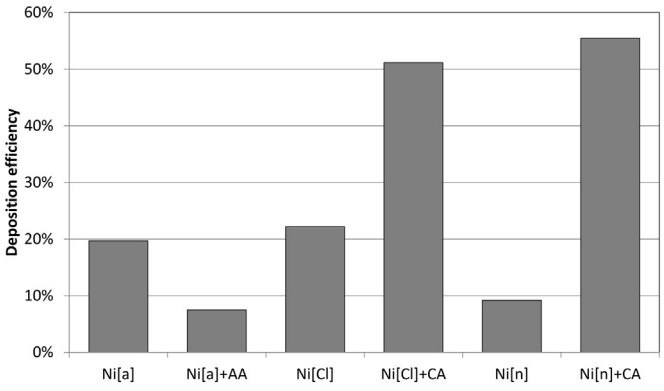

Fig. 1. Deposition efficiency for different nickel precursors.

molten or partially molten in order to adhere to the substrate upon impact. The particles must also have sufficient momentum normal to the substrate such that they are not deflected by the plasma gases near the substrate, although the threshold particle diameter for particles formed in SPPS to not turn and follow the plasma gas is not well known [29].

It has been shown that combustion of organic fuels can increase plasma enthalpy downstream of the nozzle exit, as oxygen is entrained in the plasma plume [4]. Rather than decrease the stand-off distance, which risks both the warping of and excessive oxidation of the metal substrate, a combustible fuel species was used for each of the three nickel precursors to evaluate the effect on both DE and the adhesion and cohesion of the deposited coatings.

Solutions were prepared with both Ni[Cl] and Ni[n] in which CA was added at a concentration of 1.3 M, corresponding to a citrate:nitrate ratio of 0.30. This citrate:nitrate ratio is slightly greater than the stoichiometric value of 0.28 for the combustion of Ni[n] with CA [30]. This value was chosen as a starting point and it was expected that unreacted CA would be oxidized by oxygen that is entrained within the plasma jet when spraying in open atmosphere. As shown in Fig. 1, the addition of a combustible fuel species significantly improved the DEs for both Ni[Cl] and Ni[n], which were measured to be 51% and 56%, respectively. The coatings were sufficiently well adhered that they could not be removed by scratching with a knife-edge. In contrast, however, the solution containing 1 M Ni[a] dissolved in anhydrous acetic acid had a lower DE of 8% compared to that of the aqueous solution of Ni[a] of 20%. It is possible that the enthalpy contributed by the combustion of both the acetate and acetic acid was sufficient to cause shattering of the NiO droplets [16]. Therefore, there is expected to be a limit to which the DE increases with increasing enthalpy of decomposition. The reader is referred to the following section for a discussion on the influence of the enthalpy of decomposition of the precursors on DE. Ni[a] was not evaluated further due to the comparatively low DE and poor adhesion of the deposited coatings. Based upon the higher DE obtained with Ni[n] in solution with CA compared to that obtained with Ni[Cl] in solution with CA, Ni[n] was utilized for further characterization.

3.1.1. Thermal characteristics of precursors

The thermal decomposition characteristics of precursors used to form NiO, YSZ, and composite NiO–YSZ coatings were evaluated in a simultaneous DSC–TGA experiment. The mass loss and heat flow during decomposition of the dried precursors are shown in Fig. 2. In Fig. 2(a) the decomposition processes of Ni[n] are endothermic without CA present in solution, whereas with CA addition, the two distinct decomposition processes are exothermic. Fig. 2(b) shows that the decomposition processes of the YSZ-forming precursors are slightly endothermic without CA and are exothermic with CA addition. Solutions containing both Ni[n] and YSZ-forming precursors were prepared with concentrations detailed in Table 2 under the heading NiO–YSZ (A). Fig. 2(c) shows that with CA addition, the decomposition processes are exothermic, whereas without CA addition, the decomposition processes are endothermic.

The total enthalpy of the decomposition processes, obtained by integration of the DSC curve between onset and completion of mass loss, correlates to the DE of the deposited coatings. As shown in Fig. 3, the DE increases with increasing enthalpy of decomposition for a given material set. The addition of CA to solutions containing Ni[n], YSZ-forming precursors, or a combination of Ni[n] and YSZ-forming precursors, significantly increases the enthalpy of decomposition of the precursors. The increase in DE is most significant for coatings deposited from solutions containing Ni[n], which on its own shows comparatively strong endothermic

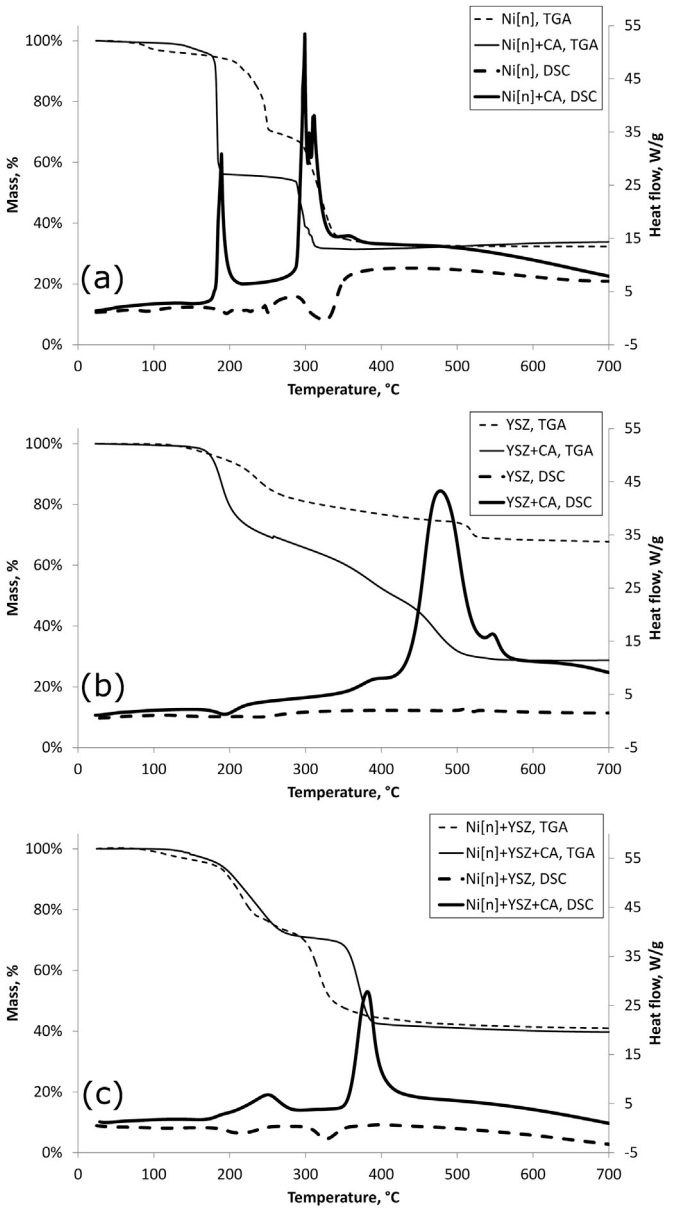

Fig. 2. TGA and DSC curves for (a) nickel(II) nitrate hexahydrate (Ni[n]) with and without citric acid (CA) addition, (b) yttrium(III) nitrate hexahydrate and zirconium dichloride oxide octahydrate, which together are abbreviated YSZ, with and without CA addition, and (c) Ni[n] and YSZ precursors with and without citric acid addition.

decomposition processes. The DE of YSZ coatings, 41%, fabricated from solutions containing CA was only slightly higher than the DE of YSZ coatings, 33%, obtained without CA addition, suggesting that the additional enthalpy contributed by combustion of CA did not significantly affect the deposition of YSZ. This result is discussed in further detail in Section 3.2.1.

3.2. Composition of Ni–YSZ coatings

The Ni content in the coating is a significant anode design parameter, as it affects the number of three phase boundaries [31], electrical conductivity [32], and tolerance to redox cycling [33] and other microstructural degradation phenomena such as Ni coarsening [34]. Therefore, the effects of torch power and stand-off distance on the Ni content of deposited coatings were evaluated in order to explore the range of manufacturable compositions of

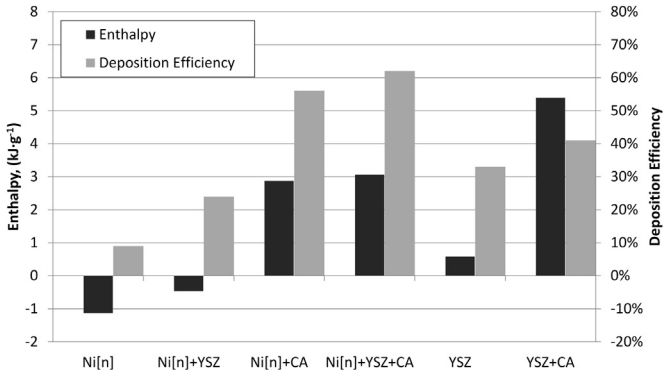

Fig. 3. Enthalpy for precursors containing Ni[n] both with and without citric acid addition obtained by integration of the heat flow curve. A positive value for enthalpy represents an exothermic process. The deposition efficiencies are for coatings fabricated from solutions containing 2 M nickel cations with Conditions A summarized in Table 1.

Ni–YSZ anodes for the set of conditions considered. A solution containing the NiO- and YSZ-forming precursors with CA addition at concentrations detailed under the heading NiO–YSZ (A) in Table 2 was used for all coatings described in this section.

Coatings were deposited using Conditions B in Table 1, where the N_2 content in the plasma varied from 30% to 80%, with a corresponding increase in torch power from 88 kW to 122 kW, respectively. The XRD spectra obtained from the as-sprayed coatings, without any post heat treatment, are shown in Fig. 4. Also shown is the spectrum obtained after heating the coating fabricated with the plasma gas containing 50% N_2 to 750 °C for 2 h in air. It is clear that both Ni and NiO are deposited in the as-sprayed coatings, and that after heat treatment in air, the Ni is fully oxidized to NiO. The intensity of the Ni peak decreases and the intensity of the NiO peak increases as the N_2 content in the plasma gas increases. Hydrogen is present in the plasma gas at a composition of 5% by volume, which could lead to partial reduction of NiO to Ni in-flight, as previously reported for the injection of NiO powders into a plasma containing H_2 [35,36].

Fig. 5(a) shows the change in NiO DE and YSZ DE with increasing torch power as a result of increasing the N_2 content of the plasma gas from 30% to 80%. Each point represents the average of three samples that were deposited in the same spray run as the coatings for which XRD spectra are shown in Fig. 4. Both Ni and NiO are deposited in the coating; therefore, the NiO DE reported in Fig. 5 is referred to the amount of NiO present in the coating after heat treatment for 2 h at 750 °C in air, after which any Ni metal present in the coating is oxidized to NiO. As the torch power increases, the YSZ DE increases while the NiO DE decreases. The YSZ DE likely increases due to increased melting of the YSZ particles at increased torch power and plasma enthalpy. The NiO DE decreases at a faster rate with respect to torch power than the YSZ DE increases, such that the volume fraction of Ni in the coating, after ex-situ reduction of NiO to Ni, decreases from 42 vol.% Ni at 88 kW to 33 vol.% Ni at 122 kW. The cause of the decreasing NiO DE reported in Fig. 5(a) is likely due to evaporation of Ni metal within the plasma. The boiling point of Ni is 2920 °C, whereas the melting temperature of YSZ is approximately 2700 °C. Therefore, if YSZ particles are reaching their melting temperature, as suggested by the increasing YSZ DE, it is likely that a fraction of the Ni particles within the plasma reach their boiling point and vaporize, rather than becoming incorporated in the coating.

Fig. 5(a) suggests that a rather narrow composition range can be fabricated, and the targeted 50 vol.% Ni corresponding to the feedstock composition was not obtained. Using less than approximately 30 vol.% N_2 with otherwise identical plasma processing parameters leads to deposition of a significant amount of amorphous material in the coatings. However, as shown in Section 3.3, the composition of the feedstock can be adjusted based on the measured NiO and YSZ DEs in order to target coatings containing a higher Ni content.

To determine the effect of stand-off distance on Ni content, Conditions B in Table 1 were used over a range of stand-off

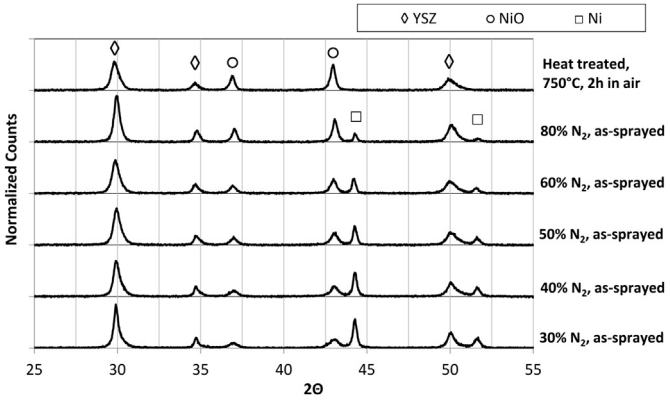

Fig. 4. XRD spectra for coatings fabricated using Conditions B in Table 1, where the N_2 content in the plasma varied from 30% to 80%. Shown at the top is the spectrum for the coating fabricated using 50% N_2, after heating to 750 °C for 2 h in air.

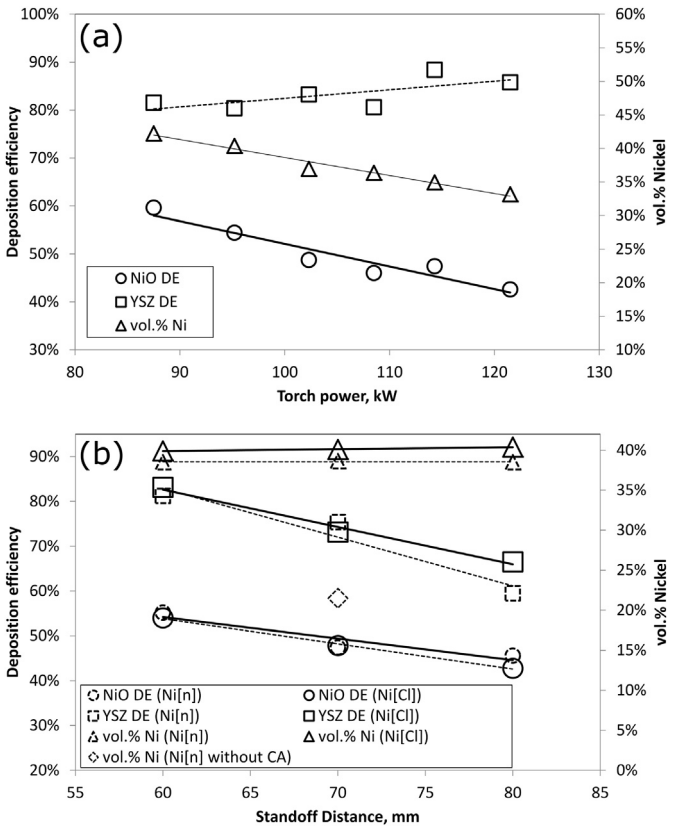

Fig. 5. NiO DE, YSZ DE, and corresponding Ni volume fraction (relative to solid content) for Ni–YSZ coatings (a) as functions of torch power and (b) as functions of stand-off distance using plasma processing Conditions B summarized in Table 1. The solution feedstock for all cases had a composition corresponding to 50 vol.% Ni after reduction of NiO to Ni. Plasma processing Conditions B were used for all coatings in (a) with the exception that the N_2 content varied from 30% to 80% in order to vary the torch power.

distances from 60 mm to 80 mm. The NiO DE, YSZ DE, and corresponding Ni content in the reduced coatings are shown in Fig. 5(b). Ni[n] and Ni[Cl], both with CA addition at concentrations as listed in Table 2, were used to compare any differences in their respective deposition characteristics. Although both the NiO DE and YSZ DE decrease with stand-off distance, the Ni content in the reduced coatings remains approximately constant for solutions fabricated using both Ni precursors. If the Ni content of the reduced coatings remains constant at stand-off distances greater than 60 mm, then the preferential loss of Ni metal due to vaporization occurs at distances less than 60 mm from the nozzle exit. Ozturk and Cetegen [37] showed that axially injected droplets precipitate at much earlier stages of the droplet lifetime compared to transversely injected droplets. This is thought to occur because the solution is injected axially into the highest temperature region of the plasma. The continued decrease in both NiO DE and YSZ DE, which occur at approximately the same rate with respect to stand-off distance between 60 mm and 80 mm, is likely due to re-solidification of each phase and/or the reduction in particle momentum normal to the substrate surface that occurs as particle velocity decreases, resulting in the particles being carried away with the plasma gas as it deflects at the substrate surface.

For comparison, Fig. 5(b) also plots the Ni content of 22 vol.% obtained for a coating fabricated at a 70 mm stand-off distance under otherwise identical conditions with the exception that the feedstock solution did not contain CA. With CA in the feedstock solution, the coating contains 39 vol.% Ni at the same stand-off distance. Potential mechanisms leading to the observed change in Ni content upon CA addition are discussed in the following section.

3.2.1. *Single stripe deposits of NiO, YSZ, and NiO–YSZ*

Fig. 6 shows deposits obtained by injecting aqueous solutions containing Ni[n] both with and without CA addition at concentrations detailed in Table 2. Single stripe deposits were obtained at stand-off distances of 40 mm and 60 mm for both solutions. Without CA addition, significantly more deposits are obtained at 40 mm compared to those obtained at 60 mm, as evident by comparison of Fig. 6(c) and (a), respectively. When CA is added to the solution, a significant increase in the amount of deposited material results, as evident by comparison of Fig. 6(b) and (a). In contrast to the significant decrease in the number of deposits obtained without CA in solution from 40 mm to 60 mm, the amount of material deposited with CA in solution does not appear to be significantly different at 40 mm and 60 mm, as shown in Fig. 6(d) and (b). Therefore, between 40 mm and 60 mm, in the absence of CA in solution, it is likely that the NiO formed has largely re-solidified and does not adhere to the substrate. These results provide insight into the large increase in DE obtained for Ni[n] solutions from 9% to 56% with the addition of CA to the solution. The combustion of CA delays re-solidification of the NiO particles formed within the plasma.

Fig. 7(a) and (b) show YSZ splats obtained at a 60 mm stand-off distance using solutions without and with CA addition, respectively, with solution concentrations detailed in Table 2. Deposits were also obtained at 40 mm (not shown); however, there did not appear to be any observable difference between the deposits collected at these two stand-off distances. The splats obtained from both solutions at 60 mm appear similar in size and shape and appear to result from fully molten YSZ droplets. Both sets of deposits from Fig. 7(a) and (b) show microcrack networks within individual splats, which likely result from thermal contraction of solidified YSZ being constrained by the metal substrate [38], and not from the shrinkage that occurs due to solvent evaporation from deposited precursor material [18].

Compared to the deposits obtained from solutions containing Ni[n], there are significantly fewer of the small spherical particles and significantly more splats with diameters on the order of a few micrometers. The mechanisms responsible for the Ni precursors leading to the formation of smaller droplets than those of the YSZ precursors are not clear from the results of this work. However, the

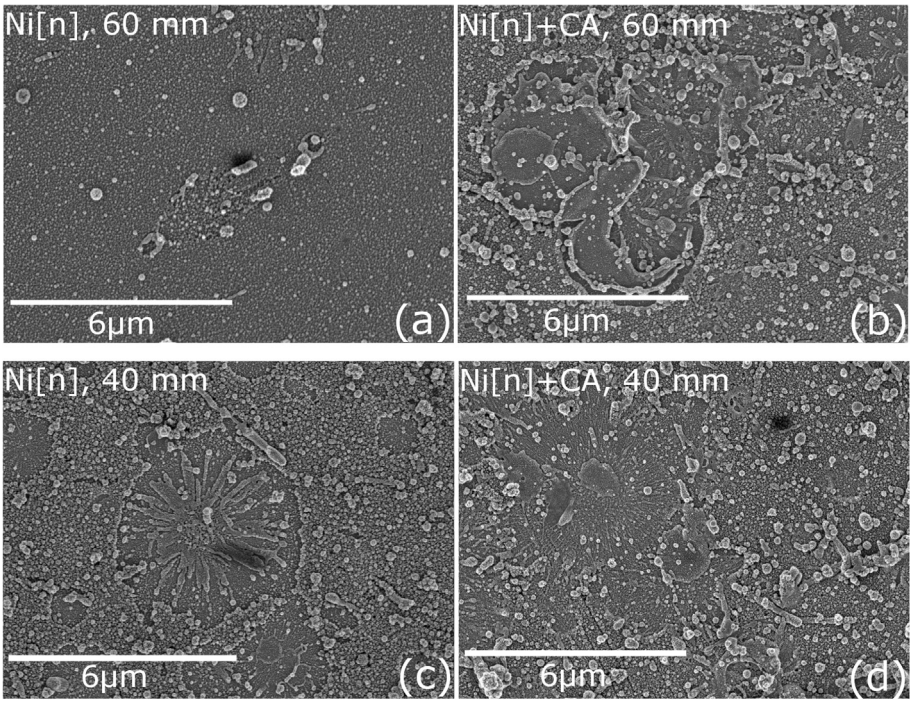

Fig. 6. Deposits from (a) Ni[n] without CA addition at a 60 mm stand-off distance, (b) Ni[n] with CA addition at a 60 mm stand-off distance, (c) Ni[n] without CA addition at a 40 mm stand-off distance, and (d) Ni[n] with CA addition at a 40 mm stand-off distance.

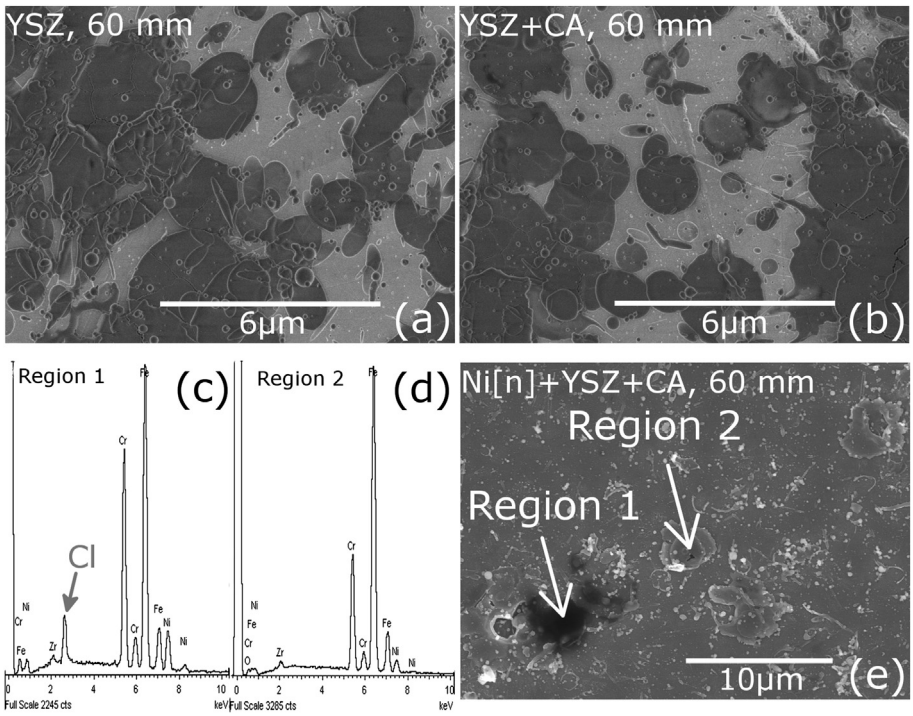

Fig. 7. Deposits of (a) YSZ without CA addition at a 60 mm stand-off distance, (b) YSZ with CA addition at a stand-off distance of 60 mm. EDS spectra for (c) region 1 and (d) region 2, as shown in (e), which shows deposits of Ni–YSZ coatings using Ni[n] with CA addition to the solution feedstock. Note that region 1 contains chlorine, resulting from incomplete synthesis of YSZ in-flight.

larger YSZ droplets that form in-flight would likely take a longer time to heat [37] than would the smaller NiO droplets. It is also expected that larger YSZ droplets attain a comparatively lower velocity, increasing their residence time and allowing the droplets to remain in a molten state at longer stand-off distances compared to the NiO particles. Therefore, CA addition to the YSZ solution does not significantly increase the DE, since the YSZ particles are otherwise in a molten state under the plasma conditions evaluated.

Single stripe deposits were also obtained using a solution containing both NiO- and YSZ-forming precursors with CA addition at a stand-off distance of 60 mm. Evidence of precursor material that had not fully formed YSZ was found, as indicated by the presence of Cl that was detected by EDS analysis, as shown in Fig. 7(c). EDS spectra obtained at locations labeled Region 1 and Region 2 in Fig. 7(e) show two regions with and without the presence of Cl, respectively. The specific mechanisms for the formation of NiO and YSZ from a single solution are not clear from this work; however, it is clear that addition of Ni[n] to the YSZ solution, even with CA addition, sufficiently decreases the plasma enthalpy such that untreated Cl-containing precursor material is deposited onto the substrate. It should also be noted that Ni[n] precursor material may also be present; however, N and O signals are ambiguous in that insufficiently treated yttrium nitrate would also produce the same signal.

3.3. Electrochemical performance

A button cell having a diameter of 2.54 cm was fabricated with the Ni–YSZ composite anode deposited on the metal support. The metal support was fabricated in house and had a sufficiently fine surface pore structure that the 23 μm ± 3 μm thick anode did not show any pin-holes when examining the surface using a scanning electron microscope. The anode was fabricated using plasma processing conditions C in Table 1. In order to obtain the targeted 50 vol.% Ni in the anode after reduction of NiO to Ni, the composition of the feedstock solution was adjusted according to that listed under the heading NiO–YSZ (B) in Table 2. These concentration adjustments are based on the measured NiO and YSZ deposition efficiencies of 48% and 75%, respectively, obtained from coatings fabricated using the same plasma processing conditions. The actual Ni content in the deposited anode was measured to be 54 vol.%, which is slightly higher than the expected 50 vol.%. At 50 vol.% Ni, the thermal expansion coefficient of the Ni–YSZ composite has been reported to be approximately 13 ppm K^{-1} [39], which is near to the value for the ferritic stainless steel used to fabricate the porous support of approximately 12 ppm K^{-1} [40].

The cell potential and power density as functions of current density are shown in Fig. 8. Performance parameters including open circuit potential, power at 0.7 V, peak power density, and polarization and series resistances are summarized in Table 3. The power density at 0.7 V and 750 °C of 448 W cm^{-2} is among the highest reported for metal supported, plasma sprayed SOFC's of similar composition and is the first set of performance data reported for any cell incorporating an anode fabricated by SPPS. This short-term performance is promising and motivates longer-term degradation testing of the stability of the anode. These studies are ongoing within our group.

3.4. Post-mortem analysis

As shown in Fig. 9(a), the Ni–YSZ anode closely follows the topography of the metal support. The sizes of the deposited NiO and YSZ particles are much smaller than the particles comprising the metal support, and therefore the anode is not capable of spanning large surface pores on the substrate. Increased surface roughness of the anode that results from defects in the surface topography of the metal support tend to lead to corresponding defects in the electrolyte layer, which lower the overall cell quality

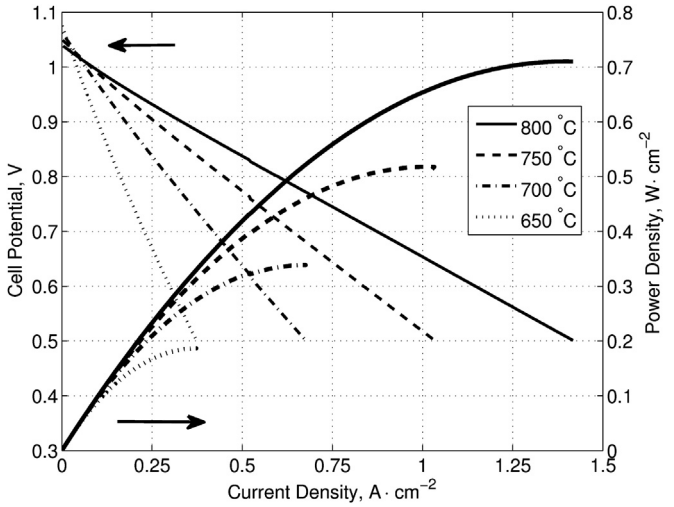

Fig. 8. Cell potential and power density as functions of current density at 800 °C, 750 °C, 700 °C, and 650 °C. Atmospheric air is fed to the cathode and humidified H_2(≈3 mol.% H_2O) is fed to the anode.

[41]. Oxidation of the metal support is visible in Fig. 9(a) and is most severe for the smallest particles, in some cases resulting in complete oxidation of the particle. Therefore, a parallel study is ongoing in our group to develop strategies to improve the long-term stability of the metal support. It is recognized that the interdiffusion of Fe, Cr, and Ni between the metal support and anode would occur over the lifetime of the SOFC and lead to performance degradation. Therefore, coating strategies to reduce the severity of interdiffusion of Fe, Cr, and Ni are also being evaluated in a parallel study.

The microstructure of the anode visible in Fig. 9(b) shows uniform mixing of the Ni and YSZ phases as well as fine-scale porosity, with pores ranging in size from sub-mircometer up to approximately 2 μm. The Ni and YSZ phases also show small microstructural features, with individual splats having a width in the cross section image up to approximately 5 μm. A quantitative description of the three dimensional structure of the anode is difficult to obtain using two dimensional cross section images, without expending the time and associated cost of detailed methods such as FIB-SEM [42] or X-ray computed tomography [43], and therefore only a brief qualitative description has been provided. The primary benefit of the SPPS process compared to conventional plasma spray processes is that it allows fabrication of Ni–YSZ anodes having smaller-sized features that are more uniformly distributed throughout the electrode, resulting in the potential for a higher three-phase boundary length per unit volume. The influence of the microstructural differences on electrochemical performance among SOFCs having anodes fabricated from a NiO–YSZ nanostructured composite powder [6], a suspension of NiO and YSZ powders [23], and a solution of NiO and YSZ-forming precursors is the subject of a forthcoming paper.

Table 3
Summary of performance parameters.

Temperature (°C)	Nernst potential (V)	OCV (V)	Power at 0.7 V W cm^{-2}	Peak power W cm^{-2}	R_s Ω cm^2	R_p at 0.7 V Ω cm^2
800	1.102	1.038	0.61	0.71	0.18	0.20
750	1.111	1.049	0.45	0.52	0.27	0.25
700	1.119	1.062	0.29	0.34	0.45	0.35
650	1.128	1.075	0.16	0.19	0.86	0.63

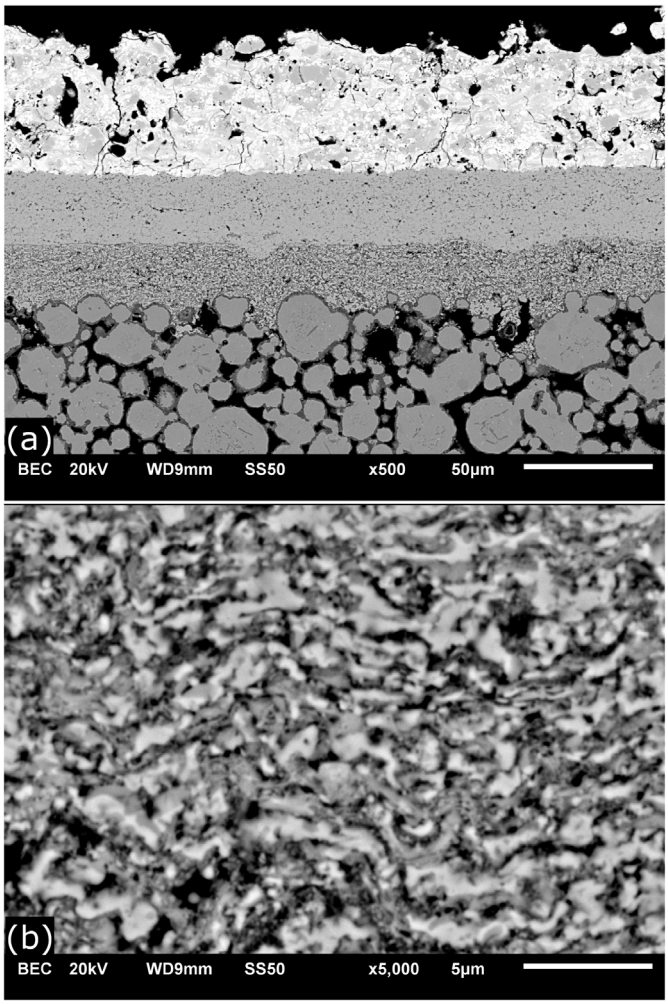

Fig. 9. (a) Cross-sectional scanning electron micrograph (backscattered electrons) of the cell showing anode fabricated by SPPS, electrolyte fabricated by SPS, and cathode fabricated by conventional atmospheric plasma spraying with a dry-powder feedstock. (b) Cross section of same cell in (a) but at an area away from the cathode, showing the anode structure.

4. Conclusions

Three different Ni precursors were evaluated including nickel(II) nitrate hexahydrate, nickel(II) chloride hexahydrate, and nickel(II) acetate tetrahydrate. Aqueous solutions at 2 M concentration led to coatings of poor quality, having low deposition efficiency and a powdery nature with poor adhesion to the substrate and poor cohesion among NiO particles comprising the coating. Addition of citric acid to the nitrate or chloride-containing solutions led to significant improvements in deposition efficiency to values greater than 50%. The improvement in deposition efficiency is likely due to the additional enthalpy contributed to the plasma by combustion of citric acid, which delays re-solidification of NiO particles.

Composite Ni–YSZ coatings were fabricated from a single aqueous solution containing NiO- and YSZ-forming precursors, to which citric acid was added as a combustible fuel species. Both Ni and NiO were deposited in the coatings. The amount of nickel incorporated in the coating, after ex-situ reduction of NiO to Ni, decreases as the torch power and plasma enthalpy increase. The decrease in nickel content of the composite coatings with increasing torch power is likely due to vaporization of nickel metal, which has a boiling point 220 °C above the melting point of YSZ.

The NiO deposition efficiency was less than the YSZ deposition efficiency for all plasma conditions evaluated, which is thought to be due to the NiO particles having a smaller size compared to the YSZ particles, which results in their earlier re-solidification or faster evaporation. There is also the potential for the smaller NiO particles to turn with the plasma gas as it is redirected near the substrate surface if the smaller mass leads to lower momentum in a direction normal to the substrate; however, this mechanism would depend on the velocities attained by each phase within the plasma.

A Ni–YSZ anode was fabricated by solution precursor plasma spraying as part of a metal-supported SOFC. The short-term cell performance including an open circuit potential of 1.05 V at 750 °C in H_2 and power density at 0.7 V of 0.45 W cm^{-2} are among the highest obtained for plasma sprayed SOFCs of similar design and materials. These are the first such data for a metal-supported cell having an anode fabricated by solution precursor plasma spraying. These results motivate further development of this spray process for fabrication of SOFC anodes as well as for evaluation of their long-term performance.

Acknowledgments

The authors gratefully acknowledge financial support from the Solid Oxide Fuel Cells Canada Strategic Research Network sponsored by NSERC and other sponsors listed at www.sofccanada.com. The authors wish to thank Michael Marr and Jeffrey Harris for developing the electrolyte and cathode layers as well as the Centre for Advanced Coating Technologies (CACT) at the University of Toronto for use of their facilities. The design and fabrication of the test station sample holder and gas delivery system by Joel Kuhn is greatly appreciated. Donation of the gasket material by Flexitallic is also appreciated.

References

[1] M.C. Tucker, J. Power Sources 195 (2010) 4570–4582.
[2] M.C. Tucker, G.Y. Lau, C.P. Jacobson, L.C. DeJonghe, S.J. Visco, J. Power Sources 175 (2008) 447–451.
[3] Y.B. Matus, L.C.D. Jonghe, C.P. Jacobson, S.J. Visco, Solid State Ionics 176 (2005) 443–449.
[4] D. Soysal, J. Arnold, P. Szabo, R. Henne, S. Ansar, J. Therm. Spray Technol. (2013) 1–11.
[5] R. Henne, J. Therm. Spray Technol. 16 (2007) 381–403.
[6] C. Metcalfe, J. Harris, J. Kuhn, M. Marr, O. Kesler, J. Therm. Spray Technol. 22 (2013) 599–608.
[7] R. Lima, A. Kucuk, C. Berndt, Mater. Sci. Eng. A 327 (2002) 224–232.
[8] M. Gell, E. Jordan, Y. Sohn, D. Goberman, L. Shaw, T. Xiao, Surf. Coat. Technol. 146–147 (2001) 48–54.
[9] L. Pawlowski, Surf. Coat. Technol. 203 (2009) 2807–2829.
[10] P. Fauchais, R. Etchart-Salas, C. Delbos, M. Tognonvi, V. Rat, J. Coudert, T. Chartier, J. Phys. D Appl. Phys. 40 (2007) 2394–2406.
[11] A. Ansar, D. Soysal, G. Schiller, Int. J. Energy Res. 33 (2009) 1191–1202.
[12] Y. Wang, J.-G. Legoux, R. Neagu, S. Hui, B. Marple, J. Therm. Spray Technol. 21 (2012) 7–15.
[13] B. Ravi, S. Sampath, R. Gambino, J. Parise, P. Devi, J. Therm. Spray Technol. 15 (2006) 701–707.
[14] N. Padture, K. Schlichting, T. Bhatia, A. Ozturk, B. Cetegen, E. Jordan, M. Gell, S. Jiang, T. Xiao, P. Strutt, E. Garca, P. Miranzo, M. Osendi, Acta Mater. 49 (2001) 2251–2257.
[15] P. Michaux, G. Montavon, A. Grimaud, A. Denoirjean, P. Fauchais, J. Therm. Spray Technol. 19 (2010) 317–327.
[16] C. Muoto, E. Jordan, M. Gell, M. Aindow, J. Therm. Spray Technol. 20 (2011) 802–816.
[17] D. Chen, E. Jordan, M. Gell, J. Mater. Sci. 42 (2007) 5576–5580.
[18] D. Chen, E.H. Jordan, M. Gell, Surf. Coat. Technol. 202 (2008) 2132–2138.
[19] G. Bertolissi, C. Chazelas, G. Bolelli, L. Lusvarghi, M. Vardelle, A. Vardelle, J. Therm. Spray Technol. 21 (2012) 1148–1162.
[20] Y. Wang, T. Coyle, J. Therm. Spray Technol. 16 (2007) 898–904.
[21] Y. Wang, T. Coyle, J. Therm. Spray Technol. 17 (2008) 692–699.
[22] X. Ma, J. Dai, H. Zhang, J. Roth, T.D. Xiao, D.E. Reisner, Trans. ASME U J. Fuel Cell Sci. Technol. 2 (2005) 190–196.
[23] C. Metcalfe, J. Kuhn, O. Kesler, J. Power Sources. 243 (2013) 172–180.
[24] H. Tu, Y. Takeda, N. Imanishi, O. Yamamoto, Solid State Ionics 117 (1999) 277–281.
[25] J. Harris, O. Kesler, ECS Trans. 35 (2011) 1927–1934.
[26] C. Metcalfe, E. Lay, O. Kesler, in: Proceedings of the International Thermal Spray Conference and Exposition, 2012, p. 885. Hamburg, Germany.
[27] R. Rampon, R.-L. Toma, G. Bertrand, C. Coddet, in: Proceedings of the International Thermal Spray Conference and Exposition, 2006, p. 682. Seattle, USA.
[28] S. Basu, B.M. Cetegen, Int. J. Heat Mass Transfer 50 (2007) 3278–3290.
[29] E. Jordan, L. Xie, M. Gell, N. Padture, B. Cetegen, A. Ozturk, X. Ma, J. Roth, T. Xiao, P. Bryant, J. Therm. Spray Technol. 13 (2004) 57–65.
[30] S. Jain, K. Adiga, V. Pai Verneker, Combust. Flame 40 (1981) 71–79.
[31] K.T. Lee, N.J. Vito, E.D. Wachsman, J. Power Sources 228 (2013) 220–228.
[32] D. Dees, T. Claar, T. Easler, D. Fee, F. Mrazek, J. Electrochem. Soc. l34 (1987) 2141–2146.
[33] D. Sarantaridis, A. Atkinson, Fuel Cells 7 (2007) 246–258.
[34] D. Simwonis, F. Tietz, D. Stöver, Solid State Ionics 132 (2000) 241–251.
[35] S. Kim, O. Kwon, S. Kumar, Y. Xiong, C. Lee, Surf. Coat. Technol. 202 (2008) 3180–3186.
[36] M. Poon, O. Kesler, J. Power Sources 210 (2012) 204–217.
[37] A. Ozturk, B.M. Cetegen, Int. J. Heat Mass Transfer 48 (2005) 4367–4383.
[38] R. McPherson, Thin Solid Films 83 (1981) 297–310.
[39] S. Aruna, M. Muthuraman, K. Patil, Solid State Ionics 111 (1998) 45–51.
[40] M. Schuisky, A. Rosberg, L. Mikkelsen, S. Linderoth, N. Christiansen, L. Gutzon, in: Proceedings of the 26th Risoe International Symposium on Materials Science, 2005, pp. 4–8.
[41] M. Marr, O. Kesler, Surf. Coat. Technol. 216 (2013) 289–296.
[42] J.R. Wilson, W. Kobsiriphat, R. Mendoza, H.-Y. Chen, J.M. Hiller, D.J. Miller, K. Thornton, P.W. Voorhees, S.B. Adler, S.A. Barnett, Nat. Mater. 5 (2006) 541–544.
[43] J.R. Izzo Jr., A.S. Joshi, K.N. Grew, W.K.S. Chiu, A. Tkachuk, S.H. Wang, W. Yun, J. Electrochem. Soc. 155 (2008) B504–B508.